THE JOURNAL OF PHYSICAL CHEMISTRY A
A JOURNAL OF THE AMERICAN CHEMICAL SOCIETY

pubs.acs.org/JPCA
Article

Solid-State High Harmonic Generation in Common Large Bandgap Substrate Materials

Published as part of The Journal of Physical Chemistry A special issue "Richard J. Saykally Festschrift".

Ezra Korican-Barlay, Bailey R. Nebgen, Jacob A. Spies,* and Michael W. Zuerch*

Cite This: J. Phys. Chem. A 2024, 128, 9337−9344
Read Online

ACCESS | Metrics & More | Article Recommendations | Supporting Information

ABSTRACT: Solid-state high harmonic generation (sHHG) spectroscopy is an emerging ultrafast technique for studying key material properties such as electronic structure at and away from equilibrium. sHHG anisotropy measurements, where sHHG spectra are recorded depending on the driving electric field relative to the crystal lattice, have become a powerful tool for studying crystal symmetries. Previous works on two-dimensional materials and other quantum materials have often used substrate-supported samples, assuming that all sHHG signals originate from the sample due to the relatively large bandgap of the substrate. While this assumption is generally reasonable, we show that some sHHG emissions from commonly used substrates can occur at moderate intensities of the sHHG driving field. In addition, we show that it is essential to consider not only the sHHG yield from a substrate but also its angular dependence relative to the material of interest. Specifically, in this work, the power-dependent and polarization angle-resolved sHHG emissions of fused silica, calcium fluoride, diamond, and sapphire of two different crystalline qualities and orientations are compared using a mid-infrared (MIR) driving field. This empirical characterization aims to guide the substrate selection for sHHG studies of novel materials to minimize the misattribution and interference of substrate-related sHHG emissions, which opens the possibility to study a wider array of materials.

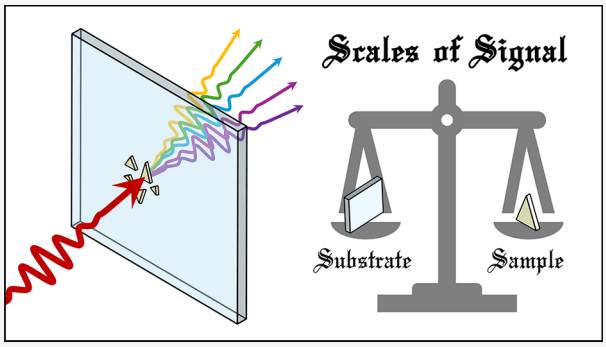

INTRODUCTION

Solid-state high harmonic generation (sHHG) spectroscopy is an emerging technique which is capable of extracting information related to the electronic structure of a material as a purely photon-based method.[1−5] sHHG spectroscopy has rapidly evolved, enabling the study of electronic and structural phase transitions, charge-spin couplings, and electronic band structures in various materials including metal oxides,[6−9] two-dimensional materials like graphene and transition metal dichalcogenides (TMDCs),[10−13] and exotic quantum materials such as Weyl semimetals and topological insulators.[14−17] In contrast to typical perturbative nonlinear optics wherein a multiphoton interaction results in harmonic generation, sHHG often follows a nonperturbative mechanism. The mechanism of nonperturbative sHHG in a material irradiated with a strong field can be understood in three steps; tunnel ionization of an electron from the valence band to the conduction band, intraband harmonic generation caused by the acceleration of carriers in the valence and conduction band generating a nonlinear current, and interband harmonic generation when the electron and hole recombine. The nontrivial interplay between perturbative and nonperturbative nonlinear processes is captured by the Keldysh parameter, which takes into account the material bandgap, driving field intensity, and driving field wavelength.[18] This technique provides critical insights into material properties, symmetry, and phase transitions by analyzing the harmonic spectra and their dependence on experimental parameters such as driving field intensity and polarization.[5,19] Critical differences of sHHG as a characterization technique for electronic structure against other more widely used photoelectron-based techniques like angle-resolved photoemission spectroscopy (ARPES) are that pristine single-crystalline samples and clean surfaces are not required for harmonic generation and measurements can be done in ambient conditions or even within complex layered systems, greatly widening its range of uses. An aspect of complementarity to techniques based on photoemission is that sHHG can probe bulk properties.

Many prior sHHG studies, particularly those focusing on two-dimensional and other quantum materials, utilize samples

Received: July 24, 2024
Revised: September 26, 2024
Accepted: September 27, 2024
Published: October 10, 2024

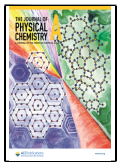

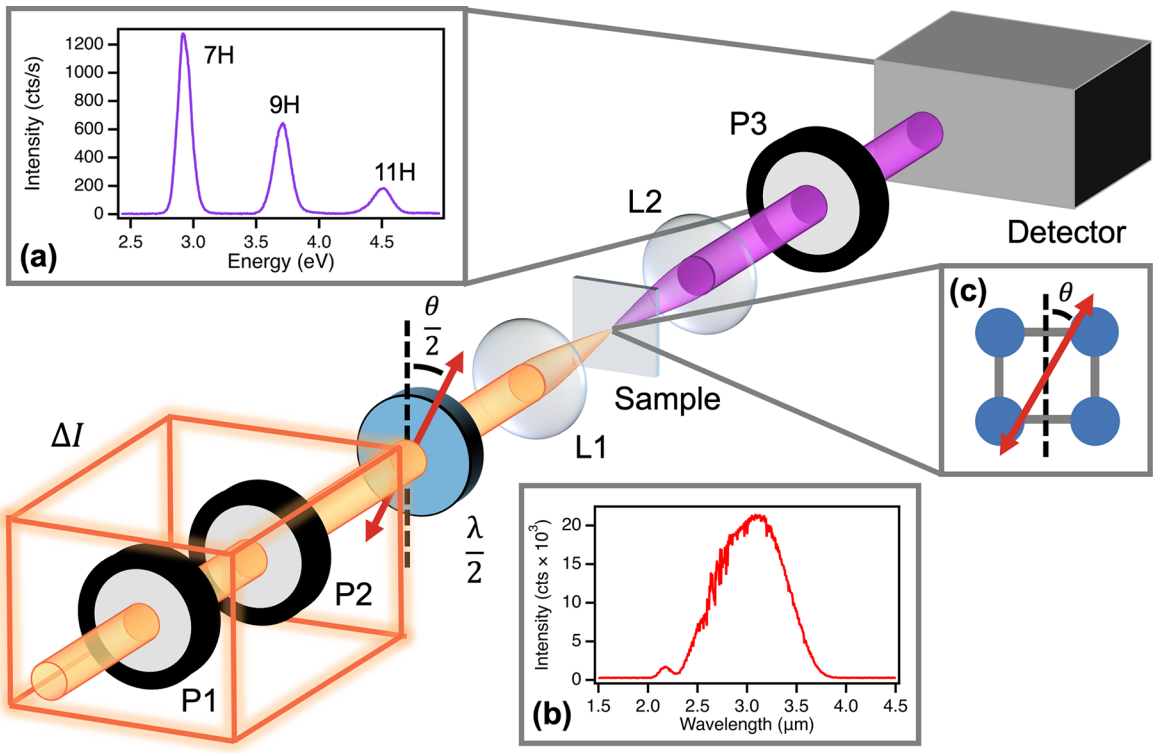

Figure 1. Schematic of optical layout used to perform solid-state high harmonic generation (sHHG) spectroscopy and anisotropy measurements. Insets: (a) Exemplary sHHG emission spectrum of a ZnO thin-film on sapphire taken with MIR intensity of ∼1.5 TW cm^{-2} under ambient conditions, (b) exemplary spectrum of the MIR driving field used for sHHG spectroscopy reported in this work, and (c) schematic of the MIR polarization (red double arrow) relative to the sample crystal axis in sHHG anisotropy measurements. Optical Components: P1−P2, MIR polarizers used for controlling the MIR intensity (ΔI); $\lambda/2$, achromatic MIR half waveplate; L1-L2, CaF_2 lenses (f_1 = 50 mm, f_2 = 25.4 mm); P3, UV−visible wire-grid polarizer for sHHG emission; θ, polarization angle.

deposited or grown on substrates that are assumed to contribute negligibly to the observed signals.[8−13,19−27] This is generally a reasonable assumption because the materials being studied, which are often small-gap materials, are mounted on large-gap insulators such as sapphire or fused silica. When the bandgap of a material of interest is much smaller than that of the insulating substrate, the tunneling rate with a mid-infrared (MIR) driving field will be higher in the material of interest and thus the sHHG efficiency will be higher, often leading to selective sHHG in the material of interest.[19] However, in larger bandgap materials of interest, higher driving field strengths are often employed to observe appreciable sHHG yield, potentially allowing sHHG to simultaneously occur in a supporting substrate material. This challenge is exacerbated when measuring sHHG anisotropies, as certain polarization angles of the driver relative to the sample crystal lattice typically result in no or very weak sHHG emission. In such cases, even weak emissions from substrates and their potentially anisotropic nature can complicate data interpretation. For example, substrates are often chosen for appropriate lattice matching with the sample. In this situation, the substrate may show the same or similar symmetry to that expected from the sample, obfuscating the desired anisotropy signal from the sample. Thus, as sHHG becomes a more widely used technique, it is necessary to understand and carefully consider substrate contributions as a factor in experimental design. Some specific aspects of sHHG interference due to propagation through bulk materials have been considered previously[28]; here we expand to focus on several common substrates and characterize their emissions as well as suggest strategies for mitigating their influence on sHHG measurements.

While the sHHG spectra of some common substrate materials have been reported, they are frequently measured using shorter near-infrared (NIR) wavelengths (∼0.8−2.0 μm) with the goal of developing vacuum ultraviolet (VUV) and extreme ultraviolet (XUV) light sources, making the magnitude of the produced signal less applicable to MIR-driven sHHG (>3 μm) performed in the context of materials characterization.[29−32] Here we address the challenge of substrate emissions by thoroughly characterizing the sHHG signal emitted by common large bandgap insulators often used as substrates under MIR driving fields. A schematic diagram of a typical sHHG spectrometer such as the one used in this work is shown in Figure 1.

We also measured MIR to UV−visible transmission of common substrates which can inform substrate choices for experiments that require sweeping the driver wavelength or measurements of harmonic emission in the deep-UV. This work seeks to provide an empirical investigation of the sHHG signal magnitude and anisotropy generated by diamond, fused silica, calcium fluoride, and sapphire (A- and C-plane) with an emphasis on informing substrate choice for future sHHG studies of supported thin films and other emerging materials.

EXPERIMENTAL METHODS

Substrate Materials and Characterization. All substrate materials were used as received without further cleaning. The dimensions of the substrates used for C-plane sapphire (AdValue Technology and MTI Corporation), A-plane

https://doi.org/10.1021/acs.jpca.4c04991
J. Phys. Chem. A 2024, 128, 9337−9344

sapphire (MTI Corporation), (100) CaF_2 (MTI Corporation), and Corning 7980 amorphous fused silica (MTI Corporation) were 10 × 10 × 0.5 mm^3. Substrate transmission spectra were collected using UV−visible spectroscopy (Shimadzu UV-2600) and Fourier transform infrared spectroscopy (Thermo Scientific Nicolet iS10).

Solid-State High Harmonic Generation Spectroscopy. The sHHG spectrometer was built around a Ti:sapphire chirped pulse amplifier (Coherent Legend Elite Duo) which produces ∼35 fs pulses with an 800 nm center wavelength, a 1 kHz repetition rate, and 13 mJ pulse energy. Approximately 5 mJ were utilized for generation of the MIR light. The pointing of the 800 nm light was corrected using an active beam stabilization system (MRC systems GmbH) before pumping an optical parametric amplifier (OPA, Light Conversion TOPAS). The signal and idler from the OPA then traveled through a noncolinear difference frequency generation stage (Light Conversion NDFG) which produced tunable MIR pulses used to perform the sHHG spectroscopy. The MIR spectrum was measured before each measurement and had a center wavelength of ∼3.1 μm (see Figure 1b).

In the sHHG apparatus (Figure 1), the MIR pulse passes through two polarizers (Thorlabs WP25M-IRA) to control the intensity and a MIR achromatic half-wave plate (B.Halle Nachfl. GmbH, Achromatic 3−6 μm) mounted in a motorized rotation stage (Thorlabs K10CR1) to control the MIR polarization prior to reaching the sample. After the sample, an analyzer polarizer (Thorlabs WP25M-UB) mounted on a motorized rotation stage (Thorlabs K10CR1) was used to perform the polarization angle-resolved sHHG measurements in both parallel and perpendicular configurations. The spectra were recorded using a spectrometer (Andor Kymera 328i) with a high-sensitivity, Peltier-cooled camera (Andor iDus DU420A-BU2).

The sHHG spectra of fused silica, sapphire, CaF_2, and diamond were measured as a function of intensity and incoming MIR polarization. The sHHG spectra were recorded at intensities between 0.055 ± 0.002 TW cm^{-2} to 3.58 ± 0.03 TW cm^{-2}. To characterize the power-dependent behavior of the sHHG spectra each harmonic peak was integrated using a trapezoidal sum, plotted logarithmically, and fit with a least-squares linear regression. The peak power density was estimated using the measured pulse energy, a spot size diameter of ∼50 μm, and a pulse duration of ∼100 fs. For the diamond, due to the significantly lower damage threshold, the pulse energy was measured before an OD 1.0 neutral density filter (Thorlabs NDIR10A) and then subsequently divided by a factor of 10 to enable more accurate measurement of the incident intensities at low fluence.

The MIR beam was focused on the back side (second surface the MIR beam passed through) of each substrate for consistency with how other samples are typically measured. This was accomplished by imaging the second surface of the substrate using a home-built inline white light microscope. Subsequently, the sHHG emission from the back surface was imaged to confirm that the emission spot was minimized in area and maximized in brightness. However, for the described experimental conditions the Rayleigh length of the MIR beam was ∼633 μm, which exceeds the substrate thickness. Therefore, we expect little deviation in the resulting sHHG emission for small errors in the focal plane in the sample.

Polarization-dependent measurements of each substrate were performed with spectra collected every 4°. The parallel polarization was measured such that the analyzer polarizer is rotated such that it is "parallel" to the incoming polarization. Similarly, the perpendicularly polarized measurements were performed with the analyzer polarizer oriented "perpendicular" to the incoming polarization. The signal was extracted from the spectra recorded at each polarization by integrating each harmonic peak using a trapezoidal sum.

RESULTS AND DISCUSSION

Substrate Transmission. A basic first consideration in choice of substrate material is transmission for both the MIR driving field used in an experiment and UV−visible harmonic emission. Figure 2 shows the transmission spectra of sapphire,

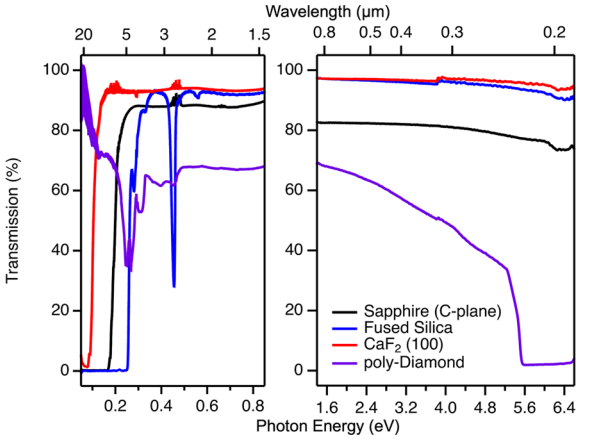

Figure 2. Measured transmission spectra of sapphire (black lines), fused silica (blue lines), (c) CaF_2 (red lines), and polycrystalline diamond (purple lines). MIR spectra are on the left and UV−visible spectra are on the right. All substrates measured were 0.5 mm thick.

fused silica, CaF_2, and diamond in both the MIR and UV−visible region. Because all three varieties of sapphire studied in this work exhibit nearly identical transmission spectra, only the C-plane substrate from MTI is shown in Figure 2. The transmission spectra for other sapphire substrates are shown in Figure S1 in the Supporting Information for completeness. In addition, an enlarged MIR transmission spectrum is plotted in Figure S2 to aid in the identification of resonance features. In the MIR spectral region, some absorption from atmospheric CO_2 and water vapor is visible which are not inherent to the substrates but to the environment in which we recorded transmission spectra. In addition, there is a small discontinuity at 3.8 eV (0.33 μm) in the UV−visible spectra that is due to a change in the used light source.

The main differences between substrate transmission spectra in the MIR region pertain to the long wavelength cutoff and the presence of resonance features, while the main differences in the UV−visible region pertain to the short wavelength cutoff. The transmission ranges of these substrates are critical in considering which substrate is best for a given sHHG measurement, potentially choosing a better MIR wavelength, or measurement geometry in order to minimize attenuation of the MIR and harmonics. The general wavelength ranges for optimal transmission of the substrates have been catalogued in Table 1.

CaF_2 exhibits the widest usable bandwidth with high transmission. Fused silica offers a similarly high transmission but is limited by a shorter wavelength cutoff (∼4.8 μm) in the

https://doi.org/10.1021/acs.jpca.4c04991
J. Phys. Chem. A 2024, 128, 9337−9344

Table 1. Summary of Materials Measured in this Work Showing Relevant Information to Aid in Substrate Choice

Substrate	Crystallinity	Observed Harmonic Orders[a]	5H Onset (TW/cm^2)	Anisotropy[b]	Literature Bandgap (eV)	Transmission Range[c]	Resonances[d]
Sapphire	C-plane	5th	0.75 ± 0.02	6-fold[e]	8.5[35]	0.2−6.2 μm	-
Sapphire	A-plane	5th, (7th)	0.77 ± 0.02	4-fold	8.5[35]	0.2−6.2 μm	-
Fused Silica	Amorphous	5th, 7th, (9th)	0.54 ± 0.02	None	-	0.2−4.8 μm	∼2.7 μm
CaF_2	(100)	5th, 7th	0.15 ± 0.02	4-fold	12.1[34]	0.2−11.9 μm	-
Diamond	Polycrystalline	5th	0.105 ± 0.002	4-fold	5.5[33]	0.3−20.0+ μm	∼5.0 μm

[a]Using the MIR spectrum shown in Figure 1b as the driver (∼3.1 μm center wavelength, 0.8 μm fwhm bandwidth). Harmonic orders that were observed but were too weak to perform a power dependent measurement are indicated in parentheses. It should be noted that observed harmonic orders are subject to change depending on specific experiment conditions. [b]Anisotropy refers to the nominal anisotropy expected in sHHG driven by a linearly polarized field based on the crystal symmetry. Splitting of symmetry features is also possible. [c]Transmission range is defined as the wavelength at which transmission drops to ∼50% before reaching zero (i.e., ignoring resonances within the bandwidth) for a 0.5 mm thick substrate. [d]Significant resonances are defined as resonances that have <50% transmission within their respective transmission range. [e]Observed only in the C-plane sapphire from MTI Corporation.

MIR and a resonance at ∼2.7 μm. Care should be taken to avoid this resonance as it can have deleterious effects on pulse dispersion that can affect sHHG efficiency. Sapphire exhibits an intermediate bandwidth with no resonance features, but lower overall transmission compared to CaF_2 and fused silica due to higher reflection losses. Diamond exhibits the lowest overall transmission and lowest high photon energy cutoff in the UV. In addition, the broad absorption centered at ∼5 μm limits the efficacy of diamond at commonly used MIR wavelengths (e.g., ∼ 3−6 μm). However, for wavelengths longer than 10 μm, diamond exhibits high transmission that would be desirable for sHHG measurements in the longer wavelength MIR and terahertz regimes.

In choosing a substrate based solely on transmission, one should consider the orientation of the sample relative to the incoming laser beam. While most of the materials above have adequate transmission in the UV−visible region, there are significant differences in the MIR transmission. For example, if the MIR driving field interacts with the sample first, the UV−visible transmission is most important because the harmonics must pass through the substrate. In contrast, if the MIR driving field passes through the substrate first, the transmission in the wavelength range of the MIR driving field should be as high as possible and resonances should be avoided.

sHHG Power Dependence of Substrate Materials. To consider how sHHG from a substrate might interfere with measurements of a material of interest, it is critical to characterize which harmonics are emitted from common substrates at what driving field strengths. Exemplary sHHG spectra measured for sapphire, fused silica, CaF_2, and diamond are shown in Figure 3. For brevity, only C-plane sapphire sourced from MTI Corporation is shown. The sHHG spectra for other suppliers and crystal orientations of sapphire are plotted in Figure S3 for completeness. Oscillations can be seen in the sHHG spectra of diamond (Figure 3a) which we qualitatively attribute to interference caused by internal reflections. There is also a minor disparity in energy of the seventh harmonic for fused silica and CaF_2 (Figure 3b) which is due to a ∼ 0.2 μm shift in the center wavelength of the MIR driving field which is within a reasonable range of fluctuation over the course of separate experiments measured over multiple days.

The power dependencies of the fifth and seventh harmonics were measured for fused silica and CaF_2 while only the power dependence of the fifth harmonic could be measured in diamond and both crystal orientations of sapphire. The ninth harmonic in fused silica and the seventh harmonic in A-plane

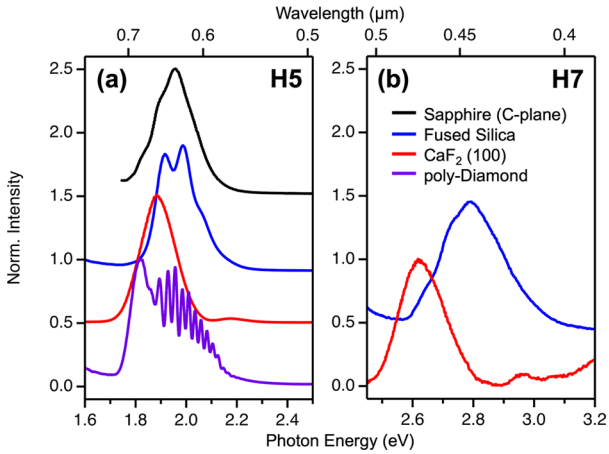

Figure 3. Exemplary sHHG spectra of the various substrates measured in this work showing (a) the 5th harmonic (**H5**) and (b) the 7th harmonic (**H7**). The spectra were normalized and offset for clarity.

sapphire were observed at higher power densities, but sample damage precluded a full power-dependent measurement. Figure 4 shows the power dependencies for fused silica, CaF_2, and polycrystalline diamond.

Figure 5 shows the power dependencies for the three sapphire substrates measured, comparing different suppliers (MTI Corporation and AdValue Technology) and crystal orientations (C-plane and A-plane). For sapphire (and polycrystalline diamond shown previously in Figure 4), only the fifth harmonic power laws were able to be measured.

The power dependencies for sapphire show clearly different regions with different power laws, deviating from the single power law expected from perturbative harmonic generation. This indicates that the harmonic emissions produced are nonperturbative as is characteristic of strong-field sHHG.

Diamond had a much lower damage threshold and produced substantial sHHG signals at lower intensities (0.105 ± 0.002 TW/cm^2) than the other measured substrates (Figure 4-5), well within the range of MIR field strengths used to study semiconductors of interest like ZnO.[9] This is consistent with diamond's bandgap being significantly smaller (5.5 eV)[33] than that of CaF_2 (12.1 eV)[34] or sapphire (8.5 eV).[35] On the other hand, fused silica had the lowest sHHG efficiency, which can be understood because the amorphous structure lacks periodicity and therefore a true band structure, limiting coherence and electron trajectories in the sHHG process.

https://doi.org/10.1021/acs.jpca.4c04991
J. Phys. Chem. A 2024, 128, 9337−9344

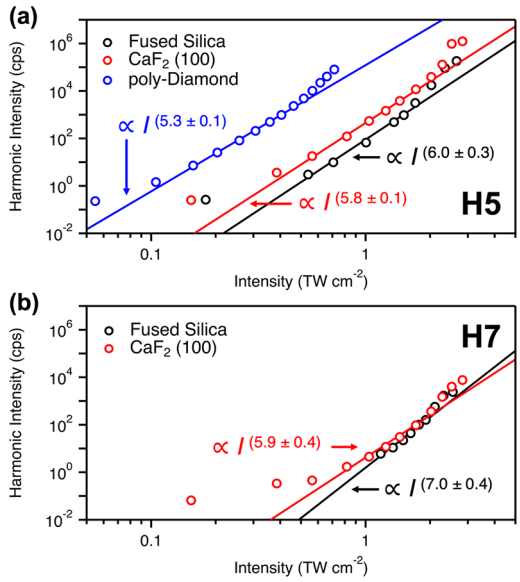

Figure 4. Power dependencies of (a) the 5th harmonic for fused silica, CaF_2 (100), and polycrystalline diamond (poly-Diamond) and (b) the 7th harmonic for fused silica and CaF_2 (100). The power laws are indicated on the plots with the error bars corresponding to the uncertainty in the fit.

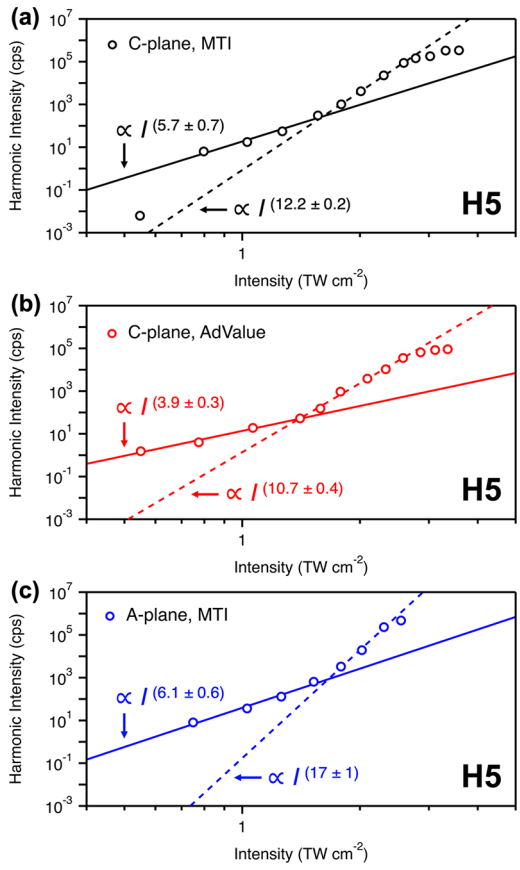

Figure 5. Power dependencies of the 5th harmonic from (a) C-plane sapphire from the MTI Corporation, (b) C-plane sapphire from AdValue Technology, and (c) A-plane sapphire from the MTI Corporation to compare different suppliers and crystal orientations. The power laws are indicated on the plots with the error bars corresponding to the uncertainty in the fit.

The low sHHG efficiency of fused silica makes it potentially an optimal substrate option for sHHG if not constrained by sample prep considerations. CaF_2 and sapphire, despite their large bandgaps, also produced significant sHHG signal at powers analogous to those at which semiconducting samples are often measured.[9]

The power dependencies observed strongly indicate that wide bandgap substrates can produce appreciable sHHG signal at MIR field strengths (0.055 ± 0.002 TW cm^{-2} to 3.58 ± 0.03 TW cm^{-2}) which are comparable to those used to measure semiconductors such as MoS_2 (1.5 TW cm^{-2})[12] and ZnO (0.6 TW cm^{-2}).[9] Therefore, it is critical to understand and characterize the sHHG emissions from common substrate materials to deconvolute their emissions from those of samples of interest. Based on the sHHG power dependencies of the substrates, one could simply be careful not to exceed the MIR powers at which a substrate emits. However, this is not feasible for all samples of interest, especially those with larger bandgaps. Another strategy based the observation of substrate sHHG emissions is to focus on the seventh harmonic and above in the sample of interest, which are easily emitted in semiconductors like ZnO (Figure 1a) but are often very weak or nonexistent in large bandgap substrates. In addition, substrate materials tend to be centrosymmetric, which means that any emission of even harmonics is disallowed in the substrate and should only be emitted from a noncentrosymmetric material of interest such as many 2D semiconductors like monolayer MoS_2. In employing these strategies to deconvolute substrate and sample sHHG, it is always critical to take a background sHHG spectrum of the substrate alone with the same MIR driver conditions to make sure that any assumptions about substrate sHHG are correct and to consider any angular dependence of sHHG emissions, which we will address in the next section.

sHHG Anisotropy of Substrate Materials. A wealth of information is contained in the sHHG anisotropy measurements of materials of interest, including symmetry and features related to the energy landscape of multiple conduction bands.[12] However, substrate materials are often single-crystalline and sometimes need to be lattice matched to a sample grown on them, meaning that anisotropic sHHG from the substrate can greatly interfere with measurements of the sample of interest. In order to deconvolute the sample and substrate sHHG anisotropy and to understand which substrates will interfere the least, we have measured the sHHG anisotropy of CaF_2 and fused silica (Figure 6) as well as C- and A-plane sapphire (Figure 7) and diamond (Figure 8) as a function of MIR driving field polarization angle. For the CaF_2, the anisotropy has 4-fold symmetry in the parallel configuration as expected based on the crystal structure; this anisotropy signal splits in the perpendicular configuration (Figure 6a). The fused silica, as expected, shows no distinct anisotropy due to its amorphous structure (Figure 6b).

The anisotropy of the A-plane sapphire also showed 4-fold symmetry which split in the perpendicular configuration (Figure 7a). In the C-plane sapphire sourced from MTI Corporation, we observe weak 6-fold symmetry in the perpendicular configuration (Figure 7b). However, the C-plane sapphire sourced from AdValue Technology does not show any discernible anisotropy (Figure 7c). This likely indicates a high dependence of the signal on the crystallinity of the substrate and indicates that not all sapphire substrates are

https://doi.org/10.1021/acs.jpca.4c04991
J. Phys. Chem. A 2024, 128, 9337−9344

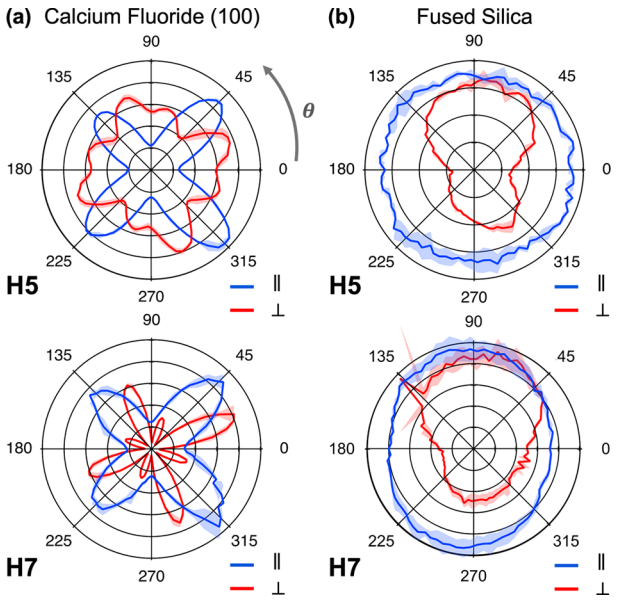

Figure 6. Parallel (blue) and perpendicular (red) anisotropy measurements for the 5th and 7th harmonics (**H5** and **H7**) of (a) calcium fluoride and (b) amorphous fused silica. Shaded regions represent the standard deviation.

equivalent, rather sHHG anisotropy signal from the substrate can be impacted by the supplier.

The diamond substrate follows a similar trend in the observed symmetry to CaF_2 and A-plane sapphire (Figure 8a) based on its unit cell crystal structure. However, because the diamond is polycrystalline, the symmetry is less pronounced than that seen in the single crystalline CaF_2. Based on the white light microscope observation of the domains in the polycrystalline diamond substrate, the size of the crystal domains (~40 μm) was comparable to the MIR spot size leading to some anisotropy still being observed when the focused MIR spot was placed carefully on a single domain (Figure 8b).

For sHHG anisotropy measurements of samples, it is critical to consider any possible signal originating from the substrate. Based on our investigation of the sHHG anisotropies of common substrate materials, it is ideal to use an amorphous substrate like fused silica in cases where lattice matching is not a significant concern. This is because, regardless of whether the substrate generates harmonics at the employed field strength, its sHHG anisotropy would not alter the symmetry of the

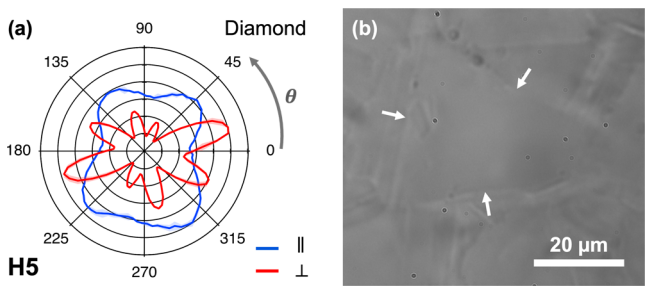

Figure 8. (a) Parallel (blue) and perpendicular (red) 5th harmonic (**H5**) anisotropy measurements of polycrystalline diamond. Shaded regions represent the standard deviation. (b) White light microscope image of measured diamond crystal domain. White arrows are included to indicate the positions of domain walls as a guide to the eye.

sHHG anisotropy measurement for the sample. Additionally, from the observed power dependence, fused silica has a moderately low harmonic efficiency in comparison to the other substrates characterized in this work which would lead to an overall reduction in the effect of the substrate's signal that is likely correctable by background subtraction. In cases where other substrates are needed for sample or driving field considerations, care can be taken to avoid harmonics emitted by substrates such as sapphire, diamond, and CaF_2 in the range of field strengths needed. In addition, polycrystalline substrates can be used to avoid contributions to anisotropy and background measurements of the substrate can be used to check and analyze contributions of the substrate to total sHHG emissions.

Table 1 summarizes the critical material characteristics for common substrate materials employed in sHHG measurements. This includes both a summary of harmonics observed and their anisotropic symmetries, as well as transmission ranges in the MIR and UV−visible regions and other important parameters.

CONCLUSIONS

In this work we have characterized the sHHG signal generated by common substrate materials. From this characterization, amorphous materials, such as fused silica, are ideal substrates to minimize impact on the measured signal, particularly in the context of polarization angle-resolved sHHG. On the other hand, fused silica specifically lacks transmission at wavelengths longer than 5 μm which renders it less ideal for experiments requiring longer driver wavelengths where the MIR passes

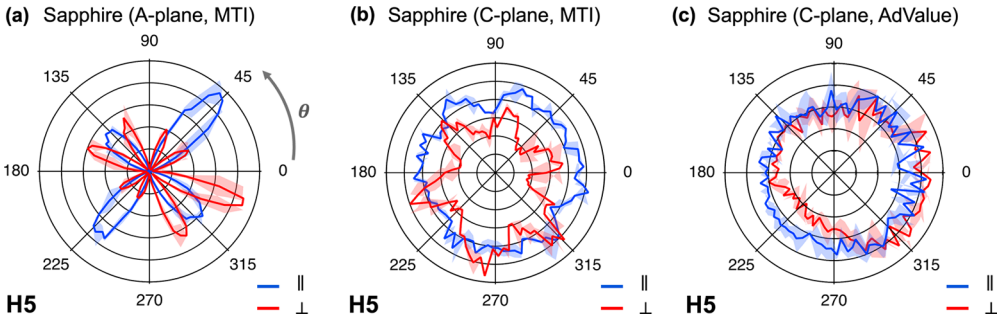

Figure 7. Parallel (blue) and perpendicular (red) anisotropy measurements of the 5th harmonic emission from (a) A-plane sapphire, (b) C-plane sapphire sourced from MTI Corporation, and (c) C-plane sapphire sourced from AdValue Technology. Shaded regions represent the standard deviation.

https://doi.org/10.1021/acs.jpca.4c04991
J. Phys. Chem. A 2024, 128, 9337−9344

through the substrate before hitting the sample. In cases when using an amorphous material is not possible for the purposes of sample preparation or insufficient MIR transmission, further thought must be given to reducing the impact of the substrate. In this case, selecting the material that produces the least sHHG signal overall or possesses different crystal symmetry than the material that can be corrected by background subtraction is ideal. Another potential option would be to use methods such as confocal imaging to remove the harmonics emitted outside of a specific focal plane, focusing studies on higher-order harmonics that are only emitted by the sample material of interest, or even harmonics which are only emitted when the sample material lacks centrosymmetry. Furthermore, one could configure these experiments in a reflection geometry which, provided that the sample thickness matches or exceeds the penetration depth of the driving field, would also remove any potential obfuscations from substrate emission. For additional technical details on reflection sHHG measurements, we refer the interested reader to prior work on this topic.[36−38] Considering substrate effects is essential to improve the reproducibility and veracity of sHHG as a technique to interrogate material properties.

■ ASSOCIATED CONTENT

Supporting Information

The Supporting Information is available free of charge at https://pubs.acs.org/doi/10.1021/acs.jpca.4c04991.

Measured MIR and UV−vis transmission spectra of sapphire comparing different suppliers and crystal orientations, full-size MIR transmission spectra of common substrate materials, sHHG spectra of sapphire comparing different suppliers and crystal orientations (PDF)

■ AUTHOR INFORMATION

Corresponding Authors

Jacob A. Spies − *Department of Chemistry, University of California, Berkeley, California 94720, United States; Materials Sciences Division, Lawrence Berkeley National Laboratory, Berkeley, California 94720, United States;* Email: jacobaspies@berkeley.edu

Michael W. Zuerch − *Department of Chemistry, University of California, Berkeley, California 94720, United States; Materials Sciences Division, Lawrence Berkeley National Laboratory, Berkeley, California 94720, United States;* orcid.org/0000-0001-5151-2119; Email: mwz@berkeley.edu

Authors

Ezra Korican-Barlay − *Department of Chemistry, University of California, Berkeley, California 94720, United States*

Bailey R. Nebgen − *Department of Chemistry, University of California, Berkeley, California 94720, United States; Materials Sciences Division, Lawrence Berkeley National Laboratory, Berkeley, California 94720, United States;* orcid.org/0000-0003-1006-7092

Complete contact information is available at: https://pubs.acs.org/10.1021/acs.jpca.4c04991

Notes

The authors declare no competing financial interest.

■ ACKNOWLEDGMENTS

E.K.B. acknowledges the support from the STEM Excellence through Equity and Diversity (SEED) Scholars Honors Program for undergraduates. B.R.N. acknowledges the funding from the National Science Foundation Graduate Research Fellowship Program (grant no. DGE 1752814). J.A.S. acknowledges the support from the Arnold O. Beckman Postdoctoral Fellowship Program. M.Z. acknowledges the funding from the W.M. Keck Foundation and funding from the UC Office of the President within the Multicampus Research Programs and Initiatives (grant no. M21PL3263) that enabled building parts of the apparatus. The authors further acknowledge funding from the National Science Foundation (grant no. NSF-DMR 2247363).

■ REFERENCES

(1) Goulielmakis, E.; Brabec, T. High Harmonic Generation in Condensed Matter. *Nat. Photonics* **2022**, *16*, 411−421.

(2) Zong, A.; Nebgen, B. R.; Lin, S.-C.; Spies, J. A.; Zuerch, M. Emerging Ultrafast Techniques for Studying Quantum Materials. *Nat. Rev. Mater.* **2023**, *8*, 224−240.

(3) Ghimire, S.; Reis, D. A. High-Harmonic Generation from Solids. *Nat. Phys.* **2019**, *15*, 10−16.

(4) Vampa, G.; McDonald, C. R.; Orlando, G.; Klug, D. D.; Corkum, P. B.; Brabec, T. Theoretical Analysis of High-Harmonic Generation in Solids. *Phys. Rev. Lett.* **2014**, *113*, No. 073901.

(5) Vampa, G.; Hammond, T. J.; Thiré, N.; Schmidt, B. E.; Légaré, F.; McDonald, C. R.; Brabec, T.; Klug, D. D.; Corkum, P. B. All-Optical Reconstruction of Crystal Band Structure. *Phys. Rev. Lett.* **2015**, *115*, No. 193603.

(6) Ghimire, S.; Dichiara, A. D.; Sistrunk, E.; Agostini, P.; Dimauro, L. F.; Reis, D. A. Observation of High-Order Harmonic Generation in a Bulk Crystal. *Nat. Phys.* **2011**, *7*, 138−141.

(7) You, Y. S.; Lu, J.; Cunningham, E. F.; Roedel, C.; Ghimire, S. Crystal Orientation-Dependent Polarization State of High-Order Harmonics. *Opt. Lett.* **2019**, *44*, 530−533.

(8) Bionta, M. R.; Haddad, E.; Leblanc, A.; Gruson, V.; Lassonde, P.; Ibrahim, H.; Chaillou, J.; Émond, N.; Otto, M. R.; Jiménez-Galán, Á.; et al. Tracking Ultrafast Solid-State Dynamics Using High Harmonic Spectroscopy. *Phys. Rev. Res.* **2021**, *3*, No. 023250.

(9) Kohrell, F.; Nebgen, B. R.; Spies, J. A.; Hollinger, R.; Zong, A.; Uzundal, C.; Spielmann, C.; Zuerch, M. A Solid-State High Harmonic Generation Spectrometer with Cryogenic Cooling. *Rev. Sci. Instrum.* **2024**, *95*, No. 023906.

(10) Yoshikawa, N.; Tamaya, T.; Tanaka, K. High-Harmonic Generation in Graphene Enhanced by Elliptically Polarized Light Excitation. *Science* **2017**, *356*, 736−738.

(11) Liu, H.; Li, Y.; You, Y. S.; Ghimire, S.; Heinz, T. F.; Reis, D. A. High-Harmonic Generation from an Atomically Thin Semiconductor. *Nat. Phys.* **2017**, *13*, 262−265.

(12) Yue, L.; Hollinger, R.; Uzundal, C. B.; Nebgen, B.; Gan, Z.; Najafidehaghani, E.; George, A.; Spielmann, C.; Kartashov, D.; Turchanin, A.; et al. Signatures of Multiband Effects in High-Harmonic Generation in Monolayer MoS_2. *Phys. Rev. Lett.* **2022**, *129*, No. 147401.

(13) Kobayashi, Y.; Heide, C.; Kelardeh, H. K.; Johnson, A.; Liu, F.; Heinz, T. F.; Reis, D. A.; Ghimire, S. Polarization Flipping of Even-Order Harmonics in Monolayer Transition-Metal Dichalcogenides. *Ultrafast Sci.* **2021**, *2021*, 1−9.

(14) Baykusheva, D.; Chacón, A.; Lu, J.; Bailey, T. P.; Sobota, J. A.; Soifer, H.; Kirchmann, P. S.; Rotundu, C.; Uher, C.; Heinz, T. F.; et al. All-Optical Probe of Three-Dimensional Topological Insulators Based on High-Harmonic Generation by Circularly Polarized Laser Fields. *Nano Lett.* **2021**, *21*, 8970−8978.

(15) Lv, Y.-Y.; Xu, J.; Han, S.; Zhang, C.; Han, Y.; Zhou, J.; Yao, S.-H.; Liu, X.-P.; Lu, M.-H.; Weng, H.; et al. High-Harmonic Generation in Weyl Semimetal β-WP_2 Crystals. *Nat. Commun.* **2021**, *12*, 6437.

(16) Schmid, C. P.; Weigl, L.; Grössing, P.; Junk, V.; Gorini, C.; Schlauderer, S.; Ito, S.; Meierhofer, M.; Hofmann, N.; Afanasiev, D.; et al. Tunable Non-Integer High-Harmonic Generation in a Topological Insulator. *Nature* **2021**, *593*, 385−390.
(17) Heide, C.; Kobayashi, Y.; Baykusheva, D. R.; Jain, D.; Sobota, J. A.; Hashimoto, M.; Kirchmann, P. S.; Oh, S.; Heinz, T. F.; Reis, D. A.; Ghimire, S. Probing Topological Phase Transitions Using High-Harmonic Generation. *Nat. Photonics* **2022**, *16*, 620−624.
(18) Kruchinin, S. Y.; Krausz, F.; Yakovlev, V. S. Colloquium: Strong-Field Phenomena in Periodic Systems. *Rev. Mod. Phys.* **2018**, *90*, No. 021002.
(19) Ndabashimiye, G.; Ghimire, S.; Wu, M.; Browne, D. A.; Schafer, K. J.; Gaarde, M. B.; Reis, D. A. Solid-State Harmonics Beyond the Atomic Limit. *Nature* **2016**, *534*, 520−523.
(20) Hollinger, R.; Herrmann, P.; Korolev, V.; Zapf, M.; Shumakova, V.; Röder, R.; Uschmann, I.; Pugžlys, A.; Baltuška, A.; Zürch, M.; et al. Polarization Dependent Excitation and High Harmonic Generation from Intense Mid-IR Laser Pulses in ZnO. *Nanomaterials* **2021**, *11*, 4.
(21) Takeda, K. S.; Uchida, K.; Nagai, K.; Kusaba, S.; Takahashi, S.; Tanaka, K. Ultrafast Electron-Electron Scattering in Metallic Phase of 2H-$NbSe_2$ Probed by High Harmonic Generation. *Phys. Rev. Lett.* **2024**, *132*, No. 186901.
(22) Bowlan, P.; Martinez-Moreno, E.; Reimann, K.; Elsaesser, T.; Woerner, M. Ultrafast Terahertz Response of Multilayer Graphene in the Nonperturbative Regime. *Phys. Rev. B* **2014**, *89*, No. 041408.
(23) Langer, F.; Hohenleutner, M.; Schmid, C. P.; Poellmann, C.; Nagler, P.; Korn, T.; Schüller, C.; Sherwin, M. S.; Huttner, U.; Steiner, J. T.; et al. Lightwave-Driven Quasiparticle Collisions on a Subcycle Timescale. *Nature* **2016**, *533*, 225−229.
(24) Taucer, M.; Hammond, T. J.; Corkum, P. B.; Vampa, G.; Couture, C.; Thiré, N.; Schmidt, B. E.; Légaré, F.; Selvi, H.; Unsuree, N.; et al. Nonperturbative Harmonic Generation in Graphene from Intense Midinfrared Pulsed Light. *Phys. Rev. B* **2017**, *96*, No. 195420.
(25) Langer, F.; Schmid, C. P.; Schlauderer, S.; Gmitra, M.; Fabian, J.; Nagler, P.; Schüller, C.; Korn, T.; Hawkins, P. G.; Steiner, J. T.; et al. Lightwave Valleytronics in a Monolayer of Tungsten Diselenide. *Nature* **2018**, *557*, 76−80.
(26) Yoshikawa, N.; Nagai, K.; Uchida, K.; Takaguchi, Y.; Sasaki, S.; Miyata, Y.; Tanaka, K. Interband Resonant High-Harmonic Generation by Valley Polarized Electron−Hole Pairs. *Nat. Commun.* **2019**, *10*, 3709.
(27) Lou, Z.; Zheng, Y.; Liu, C.; Zhang, L.; Ge, X.; Li, Y.; Wang, J.; Zeng, Z.; Li, R.; Xu, Z. Ellipticity Dependence of Nonperturbative Harmonic Generation in Few-Layer MoS_2. *Opt. Commun.* **2020**, *469*, No. 125769.
(28) Kim, Y. W.; Shao, T. J.; Kim, H.; Han, S.; Kim, S.; Ciappina, M.; Bian, X. B.; Kim, S. W. Spectral Interference in High Harmonic Generation from Solids. *ACS Photonics* **2019**, *6*, 851−857.
(29) Garejev, N.; Gražulevičiute, I.; Majus, D.; Tamošauskas, G.; Jukna, V.; Couairon, A.; Dubietis, A. Third- and Fifth-Harmonic Generation in Transparent Solids with Few-Optical-Cycle Midinfrared Pulses. *Phys. Rev. A* **2014**, *89*, No. 033846.
(30) Luu, T. T.; Garg, M.; Kruchinin, S. Y.; Moulet, A.; Hassan, M. T.; Goulielmakis, E. Extreme Ultraviolet High-Harmonic Spectroscopy of Solids. *Nature* **2015**, *521*, 498−502.
(31) Kim, H.; Han, S.; Kim, Y. W.; Kim, S.; Kim, S. W. Generation of Coherent Extreme-Ultraviolet Radiation from Bulk Sapphire Crystal. *ACS Photonics* **2017**, *4*, 1627−1632.
(32) You, Y. S.; Yin, Y.; Wu, Y.; Chew, A.; Ren, X.; Zhuang, F.; Gholam-Mirzaei, S.; Chini, M.; Chang, Z.; Ghimire, S. High-Harmonic Generation in Amorphous Solids. *Nat. Commun.* **2017**, *8*, 724.
(33) Strehlow, W. H.; Cook, E. L. Compilation of Energy Band Gaps in Elemental and Binary Compound Semiconductors and Insulators. *J. Phys. Chem. Ref. Data* **1973**, *2*, 163−200.
(34) Heaton, R. A.; Lin, C. C. Electronic Energy-Band Structure of the Calcium Fluoride Crystal. *Phys. Rev. B* **1980**, *22*, 3629−3638.
(35) Gignac, W. J.; Williams, R. S.; Kowalczyk, S. P. Valence- and Conduction-Band Structure of the Sapphire (1$\bar{1}$02) Surface. *Phys. Rev. B* **1985**, *32*, 1237−1247.
(36) Xia, P.; Kim, C.; Lu, F.; Kanai, T.; Akiyama, H.; Itatani, J.; Ishii, N. Nonlinear Propagation Effects in High Harmonic Generation in Reflection and Transmission from Gallium Arsenide. *Opt. Express* **2018**, *26*, 29393.
(37) Lu, J.; Cunningham, E. F.; You, Y. S.; Reis, D. A.; Ghimire, S. Interferometry of Dipole Phase in High Harmonics from Solids. *Nat. Photonics* **2019**, *13*, 96−100.
(38) Vampa, G.; You, Y. S.; Liu, H.; Ghimire, S.; Reis, D. A. Observation of Backward High-Harmonic Emission from Solids. *Opt. Express* **2018**, *26*, 12210−12218.

https://doi.org/10.1021/acs.jpca.4c04991
J. Phys. Chem. A 2024, 128, 9337−9344